Coatings **2015**, *5*, 124-141; doi:10.3390/coatings5020124

OPEN ACCESS

coatings

ISSN 2079-6412

www.mdpi.com/journal/coatings

Article

Influence of Experimental Parameters Using the Dip-Coating Method on the Barrier Performance of Hybrid Sol-Gel Coatings in Strong Alkaline Environments

Rita B. Figueira [1,2,*], Carlos J. R. Silva [2] and Elsa V. Pereira [1]

[1] LNEC, Laboratório Nacional de Engenharia Civil, Av. Brasil 101, 1700-066 Lisboa, Portugal; E-Mail: epereira@lnec.pt

[2] Centro de Química, Universidade do Minho, Campus de Gualtar 4710-057 Braga, Portugal; E-Mail: csilva@quimica.uminho.pt

* Author to whom correspondence should be addressed; E-Mail: rmfigueira@lnec.pt or rita@figueira.pt.

Academic Editor: Alessandro Lavacchi

Received: 20 March 2015 / Accepted: 21 April 2015 / Published: 30 April 2015

Abstract: Previous studies have shown that the barrier effect and the performance of organic-inorganic hybrid (OIH) sol-gel coatings are highly dependent on the coating deposition method as well as on the processing conditions. However, studies on how the coating deposition method influences the barrier properties in alkaline environments are scarce. The aim of this experimental research was to study the influence of experimental parameters using the dip-coating method on the barrier performance of an OIH sol-gel coating in contact with simulated concrete pore solutions (SCPS). The influence of residence time (Rt), a curing step between each dip step and the number of layers of sol-gel OIH films deposited on hot-dip galvanized steel to prevent corrosion in highly alkaline environments was studied. The barrier performance of these OIH sol-gel coatings, named U(400), was assessed in the first instants of contact with SCPS, using electrochemical impedance spectroscopy and potentiodynamic methods. The durability and stability of the OIH coatings in SCPS was monitored during eight days by macrocell current density. The morphological characterization of the surface was performed by Scanning Electronic Microscopy before and after exposure to SCPS. Glow Discharge Optical Emission Spectroscopy was used to investigate the thickness of the U(400) sol-gel coatings as a function of the number of layers deposited with and without Rt in the coatings thickness.

Keywords: sol-gel; organic-inorganic hybrid; corrosion; coatings; dipping

1. Introduction

The durability of reinforced concrete structures (RCS) is a topic of general concern due to the high costs of rehabilitation [1]. Therefore, it is of extreme importance to prevent/mitigate the corrosion of RCS exposed to aggressive environments. In these environments, the risk of corrosion is higher and the durability of RCS can only be ensured by providing additional protection to the steel reinforcement together with a correct use of high quality concrete and adequate cover [2,3].

There are several methods to improve the corrosion resistance of RCS [3–6]. In the last few years, the use of galvanized rebars has been recognized as an effective measure to increase the service life of RCS [7–10], mainly due to its low cost when compared to other protection systems [11].

The hot-dip galvanizing method is a process where a zinc layer is applied on a steel surface. The zinc acts as a barrier by hindering the contact of the aggressive agents with the steel substrate and provides cathodic protection [12,13]. Furthermore, the formed zinc corrosion products have a smaller volume than those produced from iron, thus reducing the corrosion-induced spalling of the concrete [7]. The galvanized steel reinforcement can withstand exposure to chloride ion concentrations several times higher than the chloride level that causes corrosion in steel reinforcement. Besides, the steel in concrete typically depassivates below a pH of 11.5 while galvanized reinforcement can remain passivated at a lower pH offering substantial protection against the effects of concrete carbonation [7]. These factors are accepted as the basis for improved performance of galvanized reinforcement and therefore the increase of service life of RCS compared to steel reinforcement [14]. Nevertheless, when HDGS is in contact with highly alkaline environments (fresh concrete) the zinc corrodes. This corrosion process may lead to zinc consumption until either the formation of passivation layer or until all the zinc layer is consumed [7,15–18]. To minimize this initial corrosion process, measures such as increasing the chromate content of the cement, adding water-soluble chromates into the preparation and the use of chromate conversion layers have been widely implemented. However, the use of chromates is not recommended because of the adverse health effects of the hexavalent chromium ions (Cr(VI)). Therefore, Portland cements have a limited content of Cr(VI) in their composition and the use of chromate conversion layers are currently being avoided. The research for replacement of Cr(VI) is recommended and is of concern to the scientific community. In the last few years, alternatives using sol-gel-derived coatings for improved corrosion resistance have been reported in several substrates [19].

Organic-inorganic hybrid (OIH) sol-gel coatings are a new generation of multifunctional materials where the intermolecular interactions between the macromolecular existing structures and metallic surface are of relevancy for the material properties, such as low porosity, low rigidity and adhesion to the substrate [20]. These materials can also be produced under mild conditions on an industrial scale using well established methods such as spray, dip and spin coating. Despite the advantages of these materials, constraints are present [21]. Coating complex shapes with a minimum thickness assuring a uniform, crack-free film distribution on the substrate is one of the main limitations of these materials.

This work studies the influence of three factors on the coating performance, namely residence time (Rt), cures between each deposition and the presence of more than one layer of coating. To assess the

impact on the barrier properties of the OIH coatings, considering both corrosion behaviour and economic aspects as well to get coatings with a uniform distribution, an OIH sol-gel matrix was synthesized according to the literature [22]. HDGS dip-coated with U(400) in synthetic media simulating the aqueous solution existing in the concrete pores (simulated concrete pore solution (SCPS)) was assessed by electrochemical impedance spectroscopy and potentiodynamic methods in the first instants of immersion in SCPS. Macrocell current density was used to monitor the coating durability and stability during eight days of immersion in SCPS.

The surface morphology of HDGS coated samples before exposure to the SCPS was studied by Scanning Electronic Microscopy/Energy Dispersive Spectrometry analysis and the roughness of the coatings was determined by Atomic Force Microscopy (AFM). Glow Discharge Optical Emission Spectroscopy (GD-OES) was used to obtain quantitative composition profiles to investigate the thickness of the OIH coatings as a function of the number of deposited layers and the influence of the Rt on the coating thickness.

2. Experimental Work

2.1. Reagents

A di-amino functionalized polyether (Jeffamine® D-400) provided by Fluka and 3-isocyanate propyltriethoxysilane (ICPTES, 95%, Aldrich, Munich, Germany) were stored protected from light and used as supplied. Absolute ethanol (EtOH, absolute 98%, Riedel-de-Haën, Seelze, Germany) and citric acid monohydrate (Merck, Munich, Germany) were also used as supplied. Ultra-pure water (0.055–0.060 μS/cm) obtained from a Purelab Ultra System (Elga-Enkrott, Sintra, Portugal) was used.

2.2. Sol-Gel Synthesis Procedure of Ureasilicate Coatings

Synthesis of the OIH matrices, hereafter generically referred as U(400), were performed according to the literature [22]. For the OIH coatings the 400 represents the Jeffamine® molecular weight used and "U" refers to the type of bond (urea) established between the precursors, Jeffamine® and the ICPTES.

2.3. Coating Deposition

OIH coatings were deposited on HDGS plates (5.0 × 1.0 × 0.1 cm^3) with an average Zn thickness of 16 μm on both sides, cut from commercially available sheets. HDGS coated samples were prepared by dipping the metallic substrates in the prepared mixture (sol) using a dip coater (Nima, model DC Small) at a withdrawal speed of 10 mm min^{-1}. Residence time was either nil (Rt = 0 s) or 100 s (Rt = 100 s). Samples were coated with or without Rt using one, two or three dip steps, always using the same curing conditions (15 days at 40 °C between each dipping step). Samples prepared with three consecutive dip steps without Rt were also prepared and cured in the same conditions previously stated. The curing of the coated HDGS samples was performed in an incubator-compressor (ICP-400, Memmert GmbH & Co. KG, Schwabach, Germany).

2.4. Surface Characterization

The chemical composition depth profiling of the coatings applied on the HDGS substrates was performed using a glow discharge optical emission spectrometer on coated and uncoated substrates. A LECO glow discharge GD OES 850A (LECO, St. Joseph, MI, USA) with a radiofrequency source and a 700 V RMS was used and the samples were analysed under argon atmosphere.

The morphology of the OIH sol-gel coating surface applied on HDGS specimens was analysed with a scanning electron microscope (SEM, JEOL JSM-6400, JEOS, Peabody, MA, USA) coupled with an EDS detector (Inca-xSight Oxford Instruments). The surface of the samples was covered with an ultrathin coating of gold deposited by sputter coating. SEM investigations of the surfaces were carried out by using the back-scattered electron (BSE) detector in order to emphasise the contrast for the different metallic phases. The SEM/EDS studies of the HDGS coated samples were performed on the substrate before and after 8 days of immersion in SCPS.

Atomic Force Microscopy (AFM) images were taken operating in air using the dimension NanoScope III a Controller Scanning mode: tapping mode Veeco Instruments USA, to investigate the surface morphology on the coated and uncoated HDGS surfaces before immersion in SCPS. The surface topography and roughness of the HDGS substrate before and after applying one dip step (with and without Rt), three dip steps (with Rt = 100 s) with curing processes between each deposition and three consecutive dip steps of U(400) were examined by AFM.

2.5. Electrochemical Measurements

Different electrochemical techniques were used to evaluate the barrier performance of the U(400) sol-gel coatings on HDGS in SCPS, namely: electrochemical impedance spectroscopy (EIS), potentiodynamic polarization curve and macrocell current density (i_{gal}). SCPS were prepared according to the literature [9,23] by the addition of analytical reagent grades 0.2 M KOH to a $Ca(OH)_2$ saturated solution. A final solution with a pH = 13.2 was obtained. Table 1 indicates the preparative conditions used for the deposition of the U(400) coatings on HDGS samples and the electrochemical studies performed on each sample.

Table 1. Preparative conditions and electrochemical measurements performed in each coating.

Organic-inorganic hybrid (OIH) coating U(400)		Electrochemical measurements
Coatings were cured at 40 °C for 15 days	1 Layer Rt = 0 s 1 Layer Rt = 100 s 3 Layers Rt = 0 s [a]	EIS, potentiodynamic polarization curves and i_{gal} in SCPS
Coatings were cured at 40 °C for 15 days between each layer deposited	2 Layers Rt = 0 s 2 Layers Rt = 100 s 3 Layers Rt = 0 s 3 Layers Rt = 100 s	i_{gal} in SCPS

[a] Three consecutive dip steps without Rt (only one curing period).

2.5.1. Macrocell Current Density (i_{gal})

The i_{gal} measurements were performed at room temperature on HDGS samples coated with U(400) with or without Rt (Table 1), using a system based on two parallel electrodes (rectangular metal plates with dimensions of 5.0 × 1.0 × 0.1 cm^3). As counter electrode (CE) a stainless steel (SS, type 316L) plate was used and U(400)-coated HDGS was used as a working electrode (WE). Both electrodes had an active average area of 2 cm^2. For comparison purposes, cells prepared with uncoated HDGS WE electrodes were used as a control. To assemble the electrochemical cells, SCPS was transferred to a 100 mL polyethylene flask, the electrodes were subsequently immersed and the flask closed. Using an automatic data acquisition system (DT505, series 3, Datataker, Scoresby, Australia), i_{gal} measurements of prepared cells were performed by reading the potential difference to the terminals across an external 100 Ω resistor, according to ASTM G109-07 [24]. Measurements were performed at one-minute intervals during 8 days.

2.5.2. Electrochemical Impedance Spectroscopy (EIS) and Potentiodynamic Polarization Curves Measurements

The EIS and potentiodynamic polarization curves measurements were performed at room temperature in a Faraday cage. The HDGS coated samples studied are indicated in Table 1. The EIS measurements were performed in the first instants and after 2 h of immersion in the SCPS. The potentiodynamic polarization curves were performed after 2 h and after 24 h of immersion in SCPS. A three-electrode electrochemical cell was used, consisting of a saturated calomel electrode (SCE) as a reference electrode (RE), platinum foil (exposed area ≈ 8 cm^2) as a counter electrode (CE) and coated HDGS sample as a working electrode (WE). The exposed surface area of the WE in the electrolyte was ≈ 2 cm^2. EIS studies were accomplished by applying a 20 mV (peak-to-peak, sinusoidal) electrical potential within a frequency range from 1 × 10^5 Hz to 0.01 Hz (10 points per decade) at open circuit potential (OCP). All the measurements were performed using an Impedance/Gain-Phase Analyzer (Model 1260A, Solartron-Schlumberger) and a potentiostat/galvanostat (Model 1287A, Solartron-Schlumberger) controlled by a PC using Zplot software (Solartron-Schlumberger, version 2.9c). The frequency response data of the studied electrochemical cells were displayed in a Nyquist plot, using ZView software (Solartron-Schlumberger, version 2.9c) that was also used for data fitting purposes. For comparison purposes, cells prepared with uncoated HDGS WE electrodes were used as control. The measurements were repeated two more times to check data reproducibility.

3. Results and Discussion

3.1. Surface Characterization

The depth profiling chemical composition of coatings applied on HDGS was determined by GD-OES according to ISO 16962:2005(E) [25] for each sample. The detected elements were Zn, Fe, Si and C. The thickness of the OIH was given by the difference of the depth obtained for coated and uncoated HDGS. Representative depth profiles are shown in Figure 1.

Table 2 shows the depth profile obtained for each condition studied. The thickness of U(400) was obtained from the difference between the depth found for the sample coated (zinc layer depth plus the OIH depth) and the uncoated sample (zinc layer depth). The thicknesses of the obtained U(400) coatings ranged between 2–18 µm.

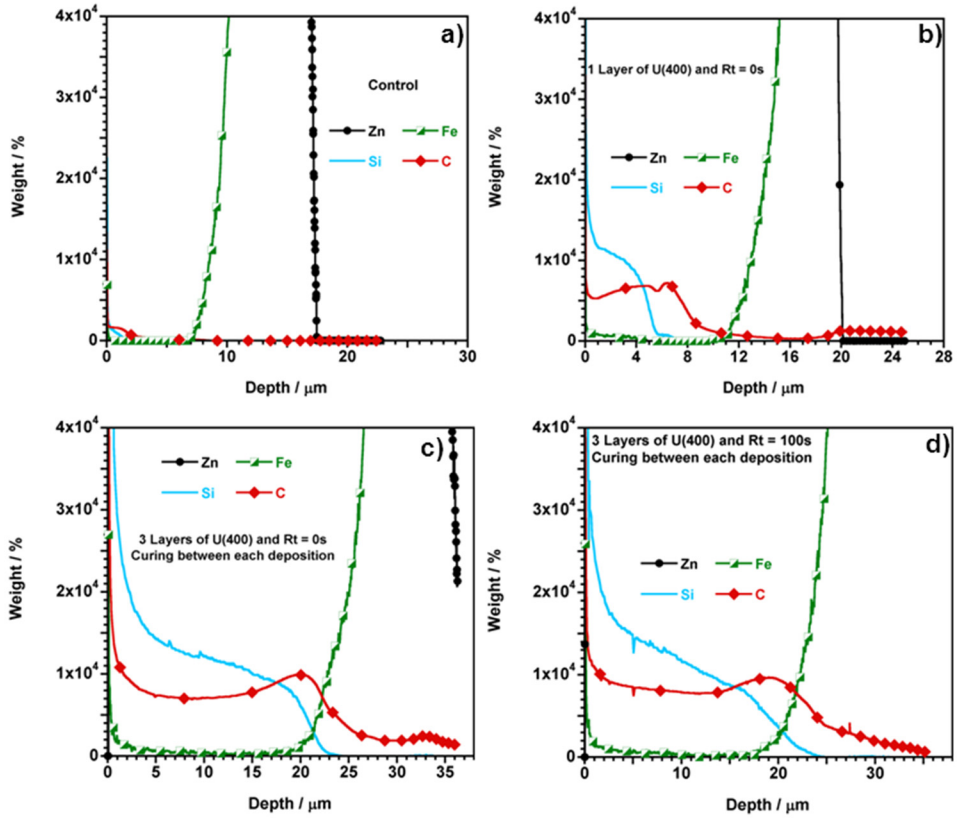

Figure 1. Detailed view of the GD-OES depth profiles for Zn, C, Fe and Si within HDGS substrates for (**a**) control; (**b**) one layer of U(400) and Rt = 0 s; (**c**) three layers of U(400) with cures between each deposition and Rt = 0 s; (**d**) three layers of U(400) with cures between each deposition and Rt = 100 s.

Table 2. Depth of OIH and zinc layer and thicknesses obtained for every condition studied.

Samples	Dipping steps	Rt/s	Depth [a]/µm (OIH + Zn layer)	OIH Thickness/µm (OIH + Zn layer) − Zn layer (control)
Uncoated HDGS (control)	–	–	19	n.a.
Coated Samples				
Curing between each deposition	1	0	21	2
	2		27	8
	3		37	18
	3 [b]		22	3
Curing between each deposition	1	100	21	2
	2		28	9
	3		36	17

[a] OIH thickness obtained according to ISO 16962:2005(E); [b] Three consecutive dip steps without Rt (only one curing period).

The thickness of the U(400) coating with two or three layers, determined according to ISO 16962:2005(E) [25] (Table 2), does not change significantly when the Rt is increased from 0 to 100 s. For the deposition of two layers with Rt = 0 s and Rt = 100 s, the thickness of U(400) increased ≈ 4 and ≈ 4.5 times compared to the thicknesses obtained for the deposition of one layer using the same Rt, respectively. Furthermore, a significant increase in the coating thickness was obtained when three layers were deposited on the substrate either with or without Rt. The coating thickness of the U(400) deposited by three dip steps, with curing between each deposition and without Rt, increased ≈ 9 times compared to the thickness obtained when one layer was deposited. The increase was ≈ 8.5 times when three layers were deposited compared to samples coated with one layer using the same Rt = 100 s.

To study the impact of the curing process between each dip-step, samples with three consecutive dip steps whitout Rt were prepared. Table 2 shows that the coating thickness obtained for samples coated by three consecutive dip steps is much smaller than the thickenss obtained for samples coated by tree dip steps with a curing process between each deposition (3 μm compared to 18 μm Rt = 0 s and 17 μm Rt = 100 s). These results indicate that to increase the thickness of an OIH coating, the curing process between each deposition is crucial. Table 2 shows that the thickness obtained for the coatings are in agreement with the number of dip steps used.

Surface morphology of coated HDGS samples was assessed by SEM/EDS analysis before immersion in SCPS for samples coated with one, two and three layers with and without Rt and cures between each deposition (Figure 2). SEM analyses revealed that U(400) coatings cover the substrate regardless the number of dip steps and whether Rt is used or not. The EDS analysis (Figure 3) shows that the lighter areas correspond the presence of Zn (surface of HDGS) and the darker areas to the presence of U(400) as these reveal high intensity peaks of C, Si and O. Figure 2 also shows that the deposition of two and three layers with cures between each deposition improves the coating distribution.

When the Rt increased to 100 s and two and three layers were deposited with cures between each dip step (Figure 2) improvements were found. However, areas barely coated were also visible. A full coverage was seldom achieved (Figures 2 and 3). These results suggest that a compromise between the time, costs and the energy consumption involved and the electrochemical performance/barrier properties of the coatings should be considered.

AFM was used to scan the surface of HDGS coated samples on an area of 10 × 10 μm^2. Figure 4 shows the topographic images before immersion in SCPS for samples coated by one dip step and three dip steps with cures between each deposition with Rt = 100 s. The most common amplitude parameters used are the average roughness (R_a) and the root mean square roughness (R_q) [26]. R_a is the arithmetic average of the absolute values of the surface height deviations measured from the mean plane within the given area and R_q is the standard deviation of the Z values within the assumed area [26]. Table 3 lists the values of R_q, R_a, and R_{max} (maximum vertical distance between the highest and lowest data points within a given area) for the control and HDGS coated samples.

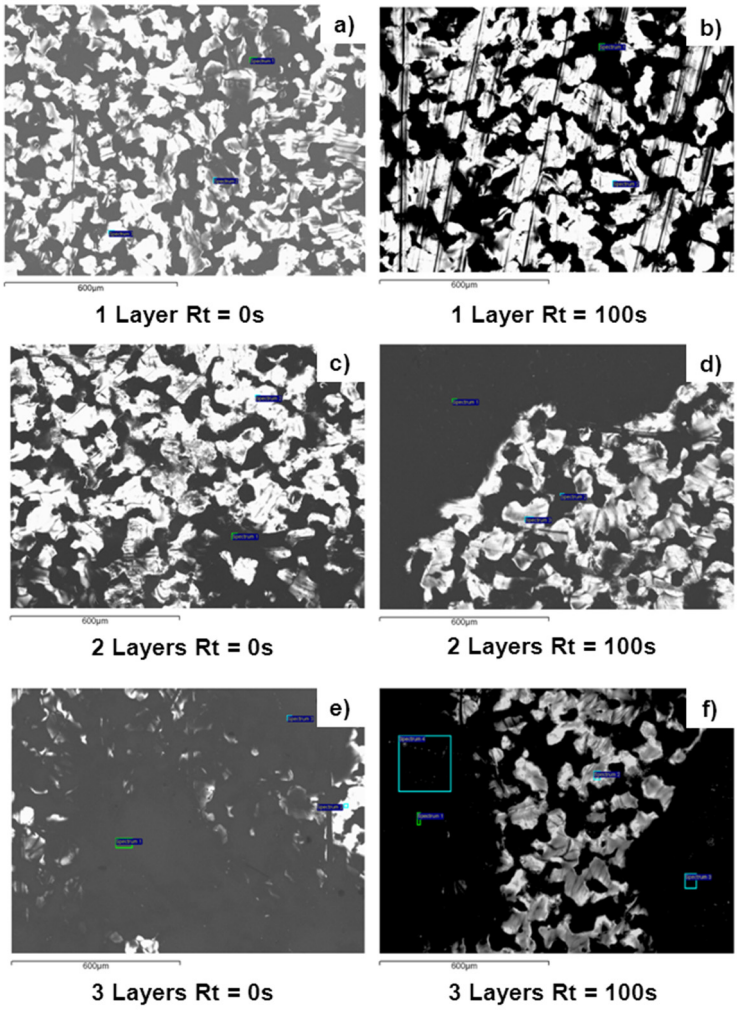

Figure 2. SEM images of HDGS sample coated with U(400): one layer (**a**) Rt = 0 s and (**b**) Rt = 100 s; two layers (**c**) Rt = 0 s and (**d**) Rt = 100 s; three layers (**e**) Rt = 0 s and (**f**) Rt = 100 s.

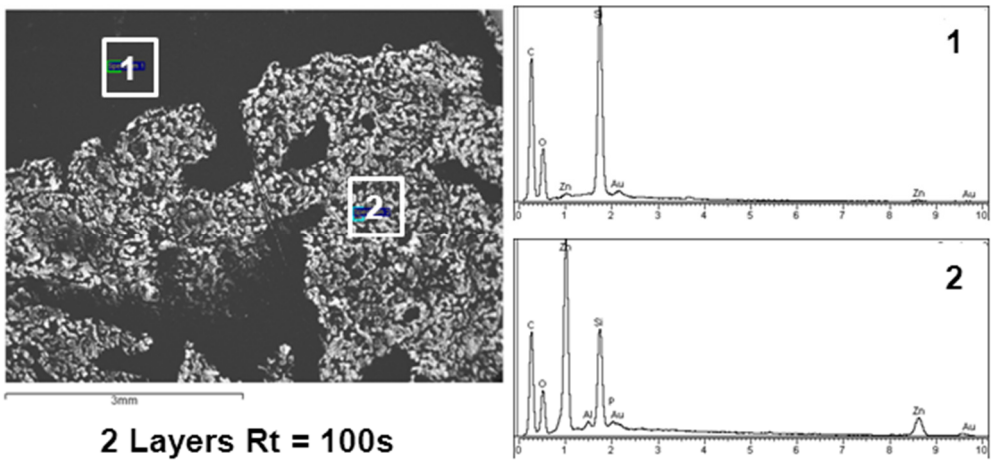

Figure 3. SEM image of HDGS coated with two layers (Rt = 100 s) of U(400). (1) and (2) represent the EDS analysis obtained in two distinct areas, which are indicated in the SEM image.

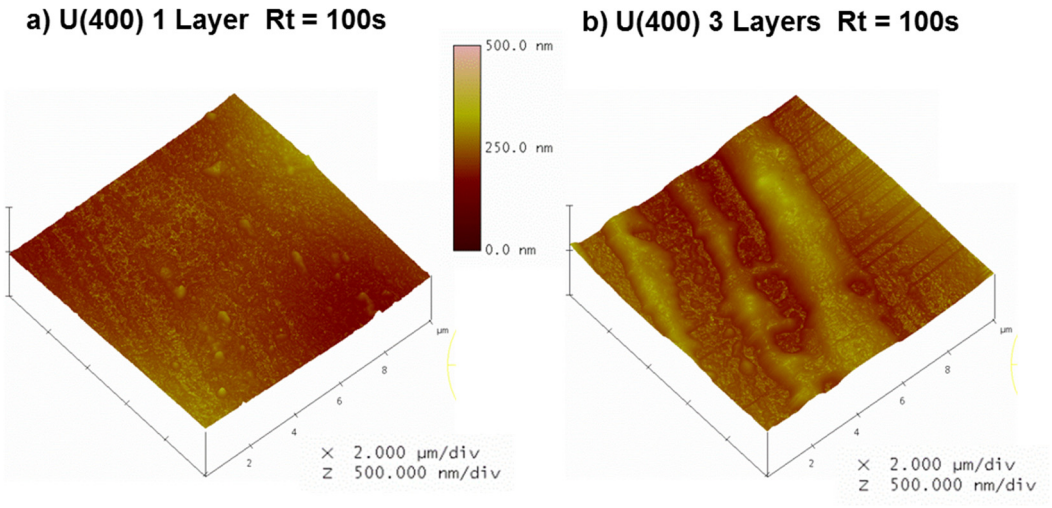

Figure 4. AFM topographic images for HDGS samples coated by: (**a**) one dip step (one layer) and (**b**) three dip steps (three layers) with cures between each deposition.

Coated samples show smoother surfaces (R_q < 37 nm) compared to the control (R_q > 100 nm). Coatings deposited by three dip steps showed areas with agglomerates (Figure 4b), compared to samples coated by one dip step (Figure 4a). However, samples coated by three layers (with or without Rt) show low R_q values compared to the ones obtained by one dip step (Rt = 0 s). Table 3 also shows that the R_q values decreased when Rt = 100 s was used, either for samples coated by one or three dip steps, and this difference was more significant for samples coated by one dip step. These results are in agreement with SEM/EDS results.

Table 3. Roughness parameters obtained for uncoated (control) and the HDGS samples coated with one and three layers.

Sample		R_q/nm	R_a/nm	R_{max}/nm
Uncoated HDGS		106	82	611
1 Layer	Rt = 0 s	36	27	330
	Rt = 100 s	17	13	135
3 Layers	Rt = 0 s [a]	28	21	243
	Rt = 100 s	23	19	153

[a] Three consecutive dip steps without Rt (only one curing period).

3.2. Electrochemical Measurements

3.2.1. Electrochemical Impedance Spectroscopy (EIS)

The EIS is technique widely used to characterize the corrosion resistance of coating systems [27,28]. EIS allows for a comparison between the performances of different systems and gives information on the evolution of the coating degradation and corrosion activity during immersion in the electrolyte. The diameter of a capacitive loop in a Nyquist diagram represents the polarization resistance of the working electrode. Therefore, larger diameters reveal improved corrosion resistance. Consequently, higher barrier protection provided by a coating corresponds to higher impedance results [29,30].

The influence of the Rt on coatings performance was studied by EIS on uncoated HDGS (control), HDGS samples coated by one dip step (with and without Rt) and by three consecutive dip steps (Rt = 0 s), in contact with SCPS. The Nyquist plots obtained for both experimental and simulated data (solid lines) at instant exposure to SCPS, once the OCP has been established (≈ 10 min), and after 2 h of immersion are shown in Figures 5 and 6. To get a more accurate fit of the experimental data, constant phase elements (CPE) instead of capacitive elements were used in all samples.

The CPE impedance is given by [30,31]:

$$Z_{\mathrm{CPE}} = \frac{1}{[Q(j\omega)^{\alpha}]} \tag{1}$$

where α and Q are parameters that are independent of the frequency [31]. When α = 1, Q represents the capacity of the interface and when α < 1, the system shows a behaviour that is associated to surface heterogeneity [31].

Three different equivalent electrical circuits (EECs) were used to fit the experimental data (Figures 5 and 6). The electrical elements R_s, $\mathrm{CPE_{dl}}$, R_{dl}, $R_{coating}$, $\mathrm{CPE_{coating}}$, R_{Oxi}, $\mathrm{CPE_{Oxi}}$ are associated, respectively, with: the electrolyte resistance, double layer capacitance at the metal–electrolyte interface, the charge transfer resistance of zinc, resistance of the sol-gel coating, capacitance of the sol-gel coating, resistance of the oxide layer and the capacitance of the oxide layer.

The CPE parameter cannot be equated to the interfacial capacitance of the OIH coatings [30,31]. To estimate the interfacial capacitance (C_{eff}) the relationship from Hirschorn *et al.* Equation (2) [32] was used, which gives the same values as Equation (3) that were proposed by Hsu and Mansfeld [33].

$$C_{\mathrm{eff}} = Q^{1/\alpha} R^{(1-\alpha)/\alpha} \tag{2}$$

$$C_{\mathrm{eff}} = Q(\omega_{\max})^{\alpha-1} \tag{3}$$

where, C_{eff} is a coating capacitance expressed in ($\mathrm{F \cdot cm^{-2}}$), Q and α are the same parameters previously mentioned. ω_{max} is the frequency at which the imaginary impedance attributed to a certain time constant has the maximum value. Fitting parameters and C_{eff} are shown in Table 4.

Control samples in the instants of exposure to SCPS are characterized by one depressed semicircle (Figure 5a). The EEC is shown in Figure 5e), which agrees with the literature [34,35]. The transfer function is represented by a resistance (R_{dl}) parallel to a CPE ($\mathrm{CPE_{dl}}$) in series with an additional resistance (R_s).

The Nyquist diagrams of coated samples exposed to SCPS (Figures 5 and 6) reveal the existence of two overlapped capacitive loops [36]. The loop at high frequencies (HF) is generally assigned to the resistance and the capacitance of the sol-gel coating ($R_{coating}$ and $\mathrm{CPE_{coating}}$ respectively). The frequency range between 0.01 and 10 Hz is assigned to the double layer capacitance ($\mathrm{CPE_{dl}}$) at the metal–electrolyte interface and to the corresponding charge transference resistance (R_{dl}) [37].

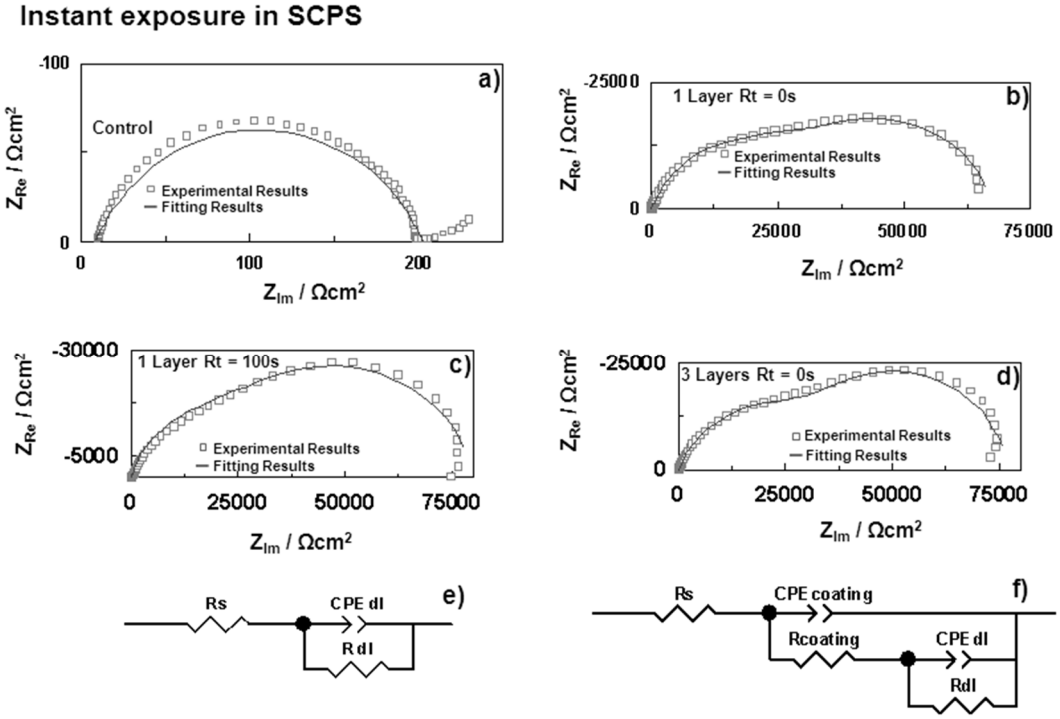

Figure 5. Nyquist plots for: (**a**) Control and U(400) coated HDGS samples by one dip step: (**b**) Rt = 0 s and (**c**) Rt = 100 s; (**d**) HDGS samples coated by three consecutive dip steps and Rt = 0 s in the instants of exposure to SCPS. EECs used for numerical fitting of the Nyquist plots for: (**e**) Control and (**f**) coated HDGS samples.

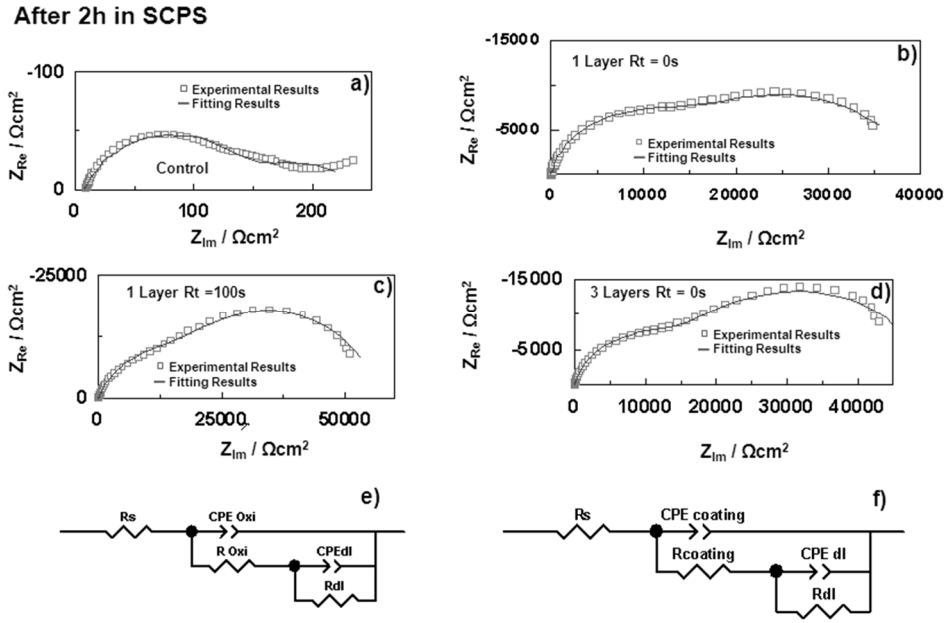

Figure 6. Nyquist plots for: (**a**) Control (uncoated HDGS) and HDGS samples coated with U(400) by one dip step; (**b**) Rt = 0 s and (**c**) Rt = 100 s; (**d**) HDGS samples coated by three consecutive dip steps and Rt = 0 s after 2 h of exposure to SCPS. EECs used for numerical fitting of the Nyquist plots for: (**e**) Control and (**f**) coated HDGS samples.

Samples coated by one and three dip steps, show in the first instants of immersion the lowest and the highest coating resistance values, respectively. A slight improvement of the coating resistance was observed when the substrate was coated by one dip step using Rt = 100 s compared to the substrate coated by one dip step without Rt. Furthermore, after 2 h of immersion, samples coated by one dip step and Rt = 100 s showed the highest coating resistance. These results suggest that the production of an appropriate coating needs time to establish the bonds between the native oxide layer of the substrate (zinc oxide) and the OIH sol (U(400)). Therefore, the introduction of the Rt during the coating deposition seems to improve the anti-corrosion behaviour of the OIH coating due to a strong interaction of free silicate groups with the metal surface and consequently increase of the resistance of the deposited coating layer.

The R_{dl} values are affected by cracks, defects or pores in the OIH coating. Therefore, this parameter, as far as the corrosion protection is concerned, is the most important. High values of R_{dl} and low values of CPE_{dl} imply improved corrosion protection and were found, in the first instants (T = 0 h) for coated HDGS samples with a Rt = 100 s (Table 4). All the coating systems show comparable responses immediately after their immersion in SCPS and after 2 h of exposure, exhibiting low capacity ($C_{coating}$) and high resistance ($R_{coating}$) (Table 4), showing a beneficial resistive behavior compared to uncoated samples.

Table 4. EIS data fitting using the EECs shown in Figures 5 and 6.

Samples		R_s ($\Omega \cdot cm^2$)	CPE_{oxide} ($s^{\alpha}\,\Omega^{-1} \cdot cm^{-2}$)	α_{oxide}	C_{oxide} ($F \cdot cm^{-2}$)	R_{oxide} ($\Omega \cdot cm^2$)	CPE_{dl} ($s^{\alpha}\,\Omega^{-1} \cdot cm^{-2}$)	α_{dl}	C_{dl} ($F \cdot cm^{-2}$)	R_{dl} ($\Omega \cdot cm^2$)
HDGS	0 h	8.29	–	–	–	–	8.74×10^{-2}	0.73	1.91×10^{-5}	1.95×10^{2}
uncoated	2 h	8.24	1.41×10^{-4}	0.74	3.39×10^{-5}	1.38×10^{2}	1.47×10^{-2}	0.50	2.08×10^{-2}	9.61×10^{1}
		OIH Coating (Layer)				*Double layer (Substrate/OIH)*				
U(400)	0 h	16.83	5.13×10^{-6}	0.78	3.21×10^{-6}	3.74×10^{4}	4.40×10^{-5}	0.89	4.53×10^{-5}	2.91×10^{4}
1 Layer Rt = 0 s	2 h	16.13	7.40×10^{-6}	0.85	5.06×10^{-6}	1.58×10^{4}	8.03×10^{-5}	0.68	1.10×10^{-5}	2.43×10^{4}
U(400)	0 h	20.76	6.29×10^{-6}	0.83	4.74×10^{-6}	4.09×10^{4}	2.54×10^{-5}	0.88	2.54×10^{-5}	3.95×10^{4}
1 Layer Rt = 100 s	2 h	23.33	1.45×10^{-5}	0.74	1.09×10^{-5}	3.01×10^{4}	6.80×10^{-5}	0.95	7.02×10^{-5}	2.69×10^{4}
U(400)	0 h	17.97	4.89×10^{-6}	0.76	3.02×10^{-6}	4.38×10^{4}	3.45×10^{-5}	0.98	3.47×10^{-5}	3.36×10^{4}
3 Layers [a]	2 h	21.13	7.26×10^{-6}	0.83	4.73×10^{-6}	1.71×10^{4}	6.66×10^{-5}	0.74	8.93×10^{-5}	3.46×10^{4}

[a] Three consecutive dip steps without Rt (only one curing period).

3.2.2. Potentiodynamic Polarization Studies

The potentiodynamic polarization studies were performed on samples coated with one layer with and without Rt, after 2 h of immersion in SCPS. Samples coated by one dip step with Rt = 0 were also studied by potentiodynamic polarization studies after 24 h of immersion in SCPS. For comparison purposes, uncoated samples (control) were also studied. The potentiodynamic polarization curves are shown in Figure 7, and Table 5 shows the electrochemical parameters obtained from potentiodynamic polarization curves. The results indicate that the U(400) films reduce the anodic and cathodic current density.

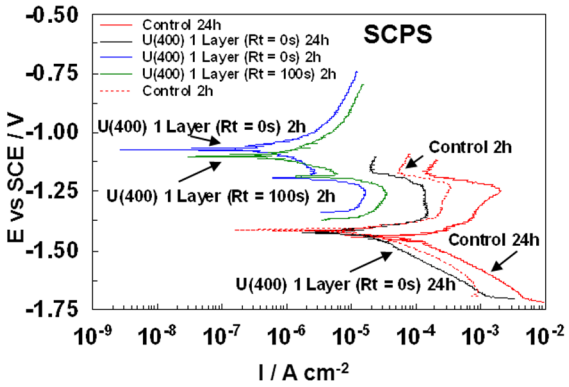

Figure 7. Potentiodynamic polarization curves obtained for HDGS coated with one layer of U(400) with Rt = 0 s and with Rt = 100 s after being immersed in SCPS for 2 h and for 24 h. The curves for uncoated HDGS after being exposed in SCPS for 2 h and 24 h were included for comparison purposes.

The protection efficiency (PE) [38] was calculated by using the following equation and is also presented in Table 5:

$$\mathrm{PE}(\%) = \frac{i_{\mathrm{corr}} - i^{*}_{\mathrm{corr}}}{i_{\mathrm{corr}}} \times 100 \quad (4)$$

where i_{corr} and i_{corr} are the corrosion current densities obtained for uncoated and coated HDGS samples, respectively.

Table 5 shows that the i_{corr} for all coated HDGS samples is lower when compared to that for the bare HDGS. For the samples immersed during 2 h in SCPS, the corrosion potential E_{corr} (−1.41 V *vs.* SCE for the bare HDGS) shows a positive shift for both coated samples with and without Rt. The value of i_{corr} for the control, after 2 h of immersion in SCPS, is ≈ 22 times higher than HDGS coated with U(400) one layer Rt = 0 s and ≈ 43 times higher than HDGS coated with U(400) one layer Rt = 100 s.

The PE obtained for the samples coated with one layer, with or without Rt, exposed to SCPS for 2 h is ≥95%. This indicates that the coating is inhibiting the anodic process, acting as a barrier to the electrolyte penetration, limiting the contact with the surface substrate. After 24 h, the PE for samples coated with one layer Rt = 0 s is above 82% (Table 5) and the i_{corr} for uncoated sample (control) is ≈ 6 times higher than HDGS coated with U(400) one layer Rt = 0 s.

Table 5. Electrochemical parameters obtained from potentiodynamic polarization curves.

Samples	ßa (V *vs.* SCE)	ßc (V *vs.* SCE)	E_{corr} (V *vs.* SCE)	i_{corr} (A·cm^{-2})	R_{p} (Ω·cm^2)	PE %
t = 2 h in SCPS						
HDGS uncoated (control)	0.101	0.035	−1.41	2.87×10^{-5}	3.90×10^{2}	–
HDGS_U(400) 1 Layer Rt = 0 s	0.045	0.319	−1.13	1.28×10^{-6}	1.33×10^{4}	96
HDGS_U(400) 1 Layer Rt = 100 s	0.059	0.115	−1.11	6.71×10^{-7}	2.54×10^{4}	98
t = 24 h in SCPS						
HDGS uncoated (control)	0.127	0.087	−1.45	9.99×10^{-5}	2.24×10^{2}	–
HDGS_U(400) 1 Layer Rt = 0 s	0.046	0.139	−1.41	1.66×10^{-5}	2.76×10^{3}	83

The electrochemical parameters obtained from potentiodynamic polarization curves indicate that the OIH coatings based on the U(400) matrix, whether or not Rt is used, mitigate the zinc corrosion in a highly alkaline environment.

3.2.3. Macrocell Current Density (i_{gal})

In order to study the coating stability over time, macrocell current density (i_{gal}) measurements were performed. Figure 8 shows the i_{gal} obtained for the electrochemical cells involving the coated HDGS samples with one, two and three layers (with and without Rt) plus the control during eight days of immersion in SCPS. During the first two days (Figure 8), the i_{gal} values measured for the control samples are much higher than the coated samples due to zinc corrosion. After two days of immersion in SCPS, an oxide layer is formed in the working electrode surface of the control samples and a decrease in the i_{gal} values is recorded. However, control samples show always higher i_{gal} values than the samples coated with U(400) regardless the number of dip steps used and whether Rt was used or not. This results are agreement with the literature [22,39]. The zinc in contact with SCPS (pH = 13.2), is oxidized and the cathodic reaction arisen from water hydrolysis with hydrogen evolution takes place on the galvanized surface [8,16,40–42]:

Anodic dissolution of zinc:

$$Zn \rightarrow Zn^{2+} + 2e^{-} \quad (5)$$

Cathodic reaction from water hydrolysis:

$$2H^{+} + 2e^{-} \rightarrow H_2 \uparrow \quad (6)$$

The global process can be described as:

$$Zn + 2H_2O \rightarrow Zn(OH)_2 + H_2 \uparrow (g) \quad (7)$$

The i_{gal} results indicate that the U(400) coatings can stand high alkaline media, and the coating barrier behaviour seems not to be affected by the high pH of the electrolyte during the period of immersion.

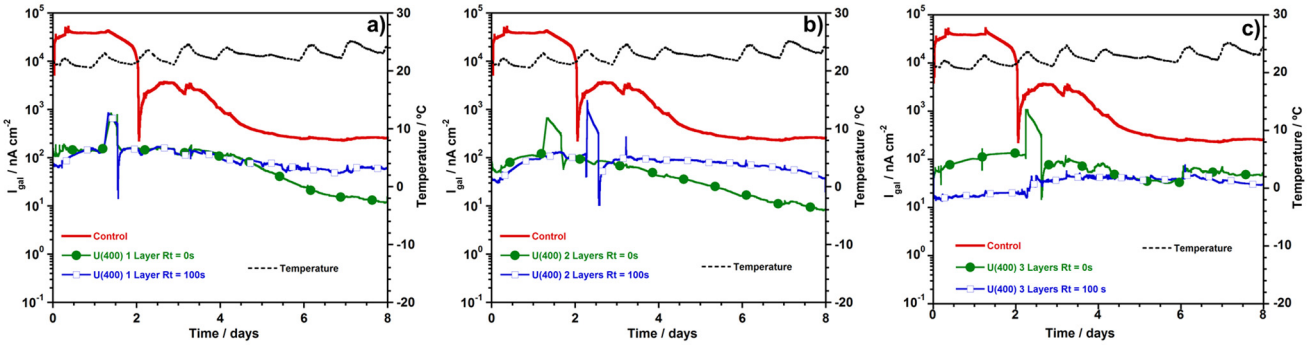

Figure 8. Plots of the variation of macrocell current density (i_{gal}) and laboratory temperature with time recorded for HDGS samples coated with U(400) (**a**) one layer (Rt = 0 s and Rt = 100 s); (**b**) two layers (Rt = 0 s and Rt = 100 s); (**c**) three layers (Rt = 0 s and Rt = 100 s) with cures between each dip step in SCPS during eight days.

4. Conlusions

The present work reports the influence of experimental parameters using the dip-coating method on the barrier performance of a hybrid sol-gel based coating namely residence time (Rt), cures between each deposition and the presence of more than one layer of coating. The coatings were deposited on HDGS by a single, double and a triple dip step method (with Rt = 0 s and Rt = 100 s, and a curing process between each deposition). The GD-OES results show that the OIH coating thickness globally increases both with the number of dipping steps and with Rt. The SEM/EDS results point to the conclusion that full coverage is seldom achieved. AFM analysis allows for the conclusion that the surface roughness of the coated samples slightly decreased when the Rt was used.

Regarding samples coated by one dip step, the EIS and the potentiodynamic data allows to conclude that when Rt = 100 s, improved performance in the first instants of immersion in SCPS was obtained. The electrochemical results obtained from monitoring cells involving HDGS coated samples, immersed in SCPS during eight days, show that regardless of the parameters used to coat the substrate, they display better performance when compared to the uncoated HDGS. Furthermore, these results allow concluding that the U(400) coatings withstand the high alkaline environment.

The results show that the implementation of several steps to coat the HDGS does not significantly improve the barrier protection. Moreover, the time consumed and the cost involved with the deposition of more than one layer is not proportional to the improvement provided on the corrosion behaviour of the substrate. The OIH coatings based on U(400) can be easily synthesized and are chemically stable in high alkaline conditions.

In conclusion, the barrier effect introduced by U(400) coatings could hinder or partially hinder the cathodic reaction involving hydrogen evolution in the very first instants of contact with SCPS and may be considered potential substitutes for chromate conversion films and systems containing Cr(VI).

Acknowledgments

The authors would like to gratefully acknowledge to Victoria Smith for assisting in the revision of the manuscript, to Ana Paula Melo for assisting in AFM analysis, the financial support from Fundação para a Ciência e Tecnologia (FCT) for the PhD grant SFRH/BD/62601/2009 and to EU COST action MP1202: HINT—"Rational design of hybrid organic-inorganic interfaces: the next step towards functional materials".

Author Contributions

R.B. Figueira, C.J.R. Silva and E.V. Pereira conceived and designed the experiments; R.B. Figueira performed the experiments; R.B. Figueira and C.J.R Silva analyzed the data; R.B. Figueira wrote the paper.

Conflicts of Interest

The authors declare no conflict of interest.

References

1. Virmani, Y.P. *Corrosion Costs and Preventive Strategies in the United States*; US Department of Transportation: Philadelphia, PA, USA, 2002; pp. 1–16.
2. Ormellese, M.; Berra, M.; Bolzoni, F.; Pastore, T. Corrosion inhibitors for chlorides induced corrosion in reinforced concrete structures. *Cem. Concr. Res.* **2006**, *36*, 536–547.
3. Böhni, H. *Corrosion in Reinforced Concrete Structures*; Woodhead Publishing Ltd.: Cambridge, UK, 2005.
4. Page, C.L.; Treadaway, K.W.J. Aspects of the electrochemistry of steel in concrete. *Nature* **1982**, *297*, 109–115.
5. Blunt, J.; Jen, G.; Ostertag, C.P. Enhancing corrosion resistance of reinforced concrete structures with hybrid fiber reinforced concrete. *Corros. Sci.* **2015**, *92*, 182–191.
6. Pereira, E.V.; Figueira, R.B.; Salta, M.M.; Fonseca, I.T.E. Long-term efficiency of two organic corrosion inhibitors for reinforced concrete. *Mater. Sci. Forum* **2010**, *636–637*, 1059–1064.
7. Yeomans, S.R. *Galvanized Steel Reinforcement in Concrete*; Elsevier: Amsterdam, The Netherlands, 2004.
8. Bellezze, T.; Malavolta, M.; Quaranta, A.; Ruffini, N.; Roventi, G. Corrosion behaviour in concrete of three differently galvanized steel bars. *Cem. Concr. Compos.* **2006**, *28*, 246–255.
9. Recio, F.J.; Alonso, M.C.; Gaillet, L.; Sánchez, M. Hydrogen embrittlement risk of high strength galvanized steel in contact with alkaline media. *Corros. Sci.* **2011**, *53*, 2853–2860.
10. Brachet, M.; Raharinaivo, M.A. Des aciers à haute résistance, galvanisés, utilisables comme armatures de béton précontraint. *Mater. Struct.* **1975**, *8*, 323–327. (In French)
11. Akamphon, S.; Sukkasi, S.; Boonyongmaneerat, Y. Reduction of zinc consumption with enhanced corrosion protection in hot-dip galvanized coatings: A process-based cost analysis. *Resour. Conserv. Recycl.* **2012**, *58*, 1–7.
12. Porter, F.C. *Corrosion Resistance of Zinc and Zinc Alloys*; CRC Press: Boca Raton, FL, USA, 1994.
13. Figueira, R.B.; Silva, C.J.R.; Pereira, E.V.; Salta, M.M. Corrosion of hot-dip galvanized steel reinforcement. *Corros. E Prot. Mater.* **2014**, *33*, 51–61.
14. Hamad, B.S.; Mike, J.A. Bond strength of hot-dip galvanized reinforcement in normal strength concrete structures. *Constr. Build. Mater.* **2005**, *19*, 275–283.
15. Macías, A.; Andrade, C. Corrosion of galvanized steel in dilute $Ca(OH)_2$ solutions (pH 11·1–12·6). *Br. Corros. J.* **1987**, *22*, 162–171.
16. Macias, A.; Andrade, C. Corrosion of galvanized steel reinforcements in alkaline solutions: Part 1: Electrochemical results. *Br. Corros. J.* **1987**, *22*, 113–118.
17. Macias, A.; Andrade, C. Corrosion of galvanized steel reinforcements in alkaline solutions: Part 2: SEM study and identification of corrosion products. *Br. Corros. J.* **1987**, *22*, 119–130.
18. Macías, A.; Andrade, C. Corrosion rate of galvanized steel immersed in saturated solutions of $Ca(OH)_2$ in the pH range 12–13·8. *Br. Corros. J.* **1983**, *18*, 82–87.
19. Figueira, R.B.; Silva, C.J.R.; Pereira, E.V. Organic–inorganic hybrid sol–gel coatings for metal corrosion protection: A review of recent progress. *J. Coat. Technol. Res.* **2014**, 1–35.

20. Balgude, D.; Sabnis, A. Sol–gel derived hybrid coatings as an environment friendly surface treatment for corrosion protection of metals and their alloys. *J. Sol-Gel Sci. Technol.* **2012**, *64*, 124–134.
21. Guglielmi, M. Sol-gel coatings on metals. *J. Sol-Gel Sci. Technol.* **1997**, *8*, 443–449.
22. Figueira, R.B.; Silva, C.J.; Pereira, E.V.; Salta, M.M. Ureasilicate hybrid coatings for corrosion protection of galvanized steel in cementitious media. *J. Electrochem. Soc.* **2013**, *160*, C467–C479.
23. Sánchez, M.; Alonso, M.C.; Cecílio, P.; Montemor, M.F.; Andrade, C. Electrochemical and analytical assessment of galvanized steel reinforcement pre-treated with Ce and La salts under alkaline media. *Cem. Concr. Compos.* **2006**, *28*, 256–266.
24. *ASTM G109 Test Method for Determining Effects of Chemical Admixtures on Corrosion of Embedded Steel Reinforcement in Concrete Exposed to Chloride Environments*; ASTM International: West Conshohocken, PA, USA, 2007.
25. *ISO 16962:2005 Surface Chemical Analysis—Analysis of Zinc- and/or Aluminium-Based Metallic Coatings by Glow-Discharge Optical-Emission Spectrometry*; ISO: Geneva, Switzerland, 2005.
26. Khulbe, K.C.; Feng, C.Y.; Matsuura, T. *Synthetic Polymeric Membranes*; Springer Laboratory; Springer Berlin Heidelberg: Berlin, Heidelberg, Germany, 2008.
27. Zheludkevich, M.L.; Yasakau, K.A.; Bastos, A.C.; Karavai, O.V.; Ferreira, M.G.S. On the application of electrochemical impedance spectroscopy to study the self-healing properties of protective coatings. *Electrochem. Commun.* **2007**, 2622–2628.
28. Arthanareeswari, M.; Narayanan, T.S.N.S.; Kamaraj, P.; Tamilselvi, M. Polarization and impedance studies on zinc phosphate coating developed using galvanic coupling. *J. Coat. Technol. Res.* **2012**, *9*, 39–46.
29. Lamaka, S.V.; Zheludkevich, M.L.; Yasakau, K.A.; Serra, R.; Poznyak, S.K.; Ferreira, M.G.S. Nanoporous titania interlayer as reservoir of corrosion inhibitors for coatings with self-healing ability. *Prog. Org. Coat.* **2007**, *58*, 127–135.
30. Barsoukov, E.; Macdonald, J.R. *Impedance Spectroscopy: Theory, Experiment, and Applications*, 2nd Ed.; Wiley: Hoboken, NJ, USA, 2005.
31. Orazem, M.E.; Tribollet, B. *Electrochemical Impedance Spectroscopy*; Wiley: Hoboken, NJ, USA, 2008.
32. Hirschorn, B.; Orazem, M.E.; Tribollet, B.; Vivier, V.; Frateur, I.; Musiani, M. Determination of effective capacitance and film thickness from constant-phase-element parameters. *Electrochim. Acta* **2010**, *55*, 6218–6227.
33. Hsu, C.H.; Mansfeld, F. Technical note: concerning the conversion of the constant phase element parameter Y0 into a capacitance. *Corrosion* **2001**, *57*, doi:10.5006/1.3280607.
34. Lebrini, M.; Fontaine, G.; Gengembre, L.; Traisnel, M.; Lerasle, O.; Genet, N. Corrosion behaviour of galvanized steel and electroplating steel in aqueous solution: AC impedance study and XPS. *Appl. Surf. Sci.* **2008**, *254*, 6943–6947.
35. Lebrini, M.; Fontaine, G.; Gengembre, L.; Traisnel, M.; Lerasle, O.; Genet, N. Corrosion protection of galvanized steel and electroplating steel by decanoïc acid in aqueous solution: Electrochemical impedance spectroscopy, XPS and ATR-FTIR. *Corros. Sci.* **2009**, *51*, 1201–1206.

36. Corfias, C.; Pebere, N.; Lacabanne, C. Characterization of a thin protective coating on galvanized steel by electrochemical impedance spectroscopy and a thermostimulated current method. *Corros. Sci.* **1999**, *41*, 1539–1555.
37. Hamlaoui, Y.; Tifouti, L.; Pedraza, F. Corrosion behaviour of molybdate–phosphate–silicate coatings on galvanized steel. *Corros. Sci.* **2009**, *51*, 2455–2462.
38. Ahmad, S.; Zafar, F.; Sharmin, E.; Garg, N.; Kashif, M. Synthesis and characterization of corrosion protective polyurethanefattyamide/silica hybrid coating material. *Prog. Org. Coat.* **2012**, *73*, 112–117.
39. Figueira, R.M.; Pereira, E.V.; Silva, C.J.R.; Salta, M.M. Corrosion protection of hot dip galvanized steel in mortar. *Port. Electrochim. Acta* **2013**, *31*, 277–287.
40. González, J.A.; Vazquez, A.J. Effect of four coating structures on corrosion kinetic of galvanized reinforcement in concrete. *Matér. Constr.* **1984**, *17*, 409–414.
41. Everett, L.H.; Treadaway, K.W.J. *The Use of Galvanised Steel Reinforcement in Building*; Building Research Station, Ministry of Public Building and Works: Garston, UK, 1970.
42. Andrade, M.C.; Macias, A. Galvanized Reinforcements in Concrete. In *Surface Coatings—2*; Wilson, A.D., Nicholson, J.W., Prosser, H.J., Eds.; Springer: Dordrecht, The Netherlands, 1988; pp. 137–182.